crystals

MDPI

Article

Iron Bonding with Light Elements: Implications for Planetary Cores Beyond the Binary System

Hong Yang [1,*], Wenzhong Wang [2] and Wendy L. Mao [1,3,*]

[1] Department of Earth and Planetary Sciences, Doerr School of Sustainability, Stanford University, Stanford, CA 94305, USA
[2] School of Earth and Space Sciences, University of Science and Technology of China, Hefei 230026, China; wwz@ustc.edu.cn
[3] SLAC National Accelerator Laboratory, Menlo Park, CA 94025, USA
* Correspondence: hyang777@stanford.edu (H.Y.); wmao@stanford.edu (W.L.M.)

Abstract: Light element alloying in iron is required to explain density deficit and seismic wave velocities in Earth's core. However, the light element composition of the Earth's core seems hard to constrain as nearly all light element alloying would reduce the density and sound velocity (elastic moduli). The alloying light elements include oxidizing elements like oxygen and sulfur and reducing elements like hydrogen and carbon, yet their chemical effects in the alloy system are less discussed. Moreover, Fe-X-ray Absorption Near Edge Structure (Fe-XANES) fingerprints have been studied for silicate materials with ferrous and ferric ions, while not many X-ray absorption spectroscopy (XAS) studies have focused on iron alloys, especially at high pressures. To investigate the bonding nature of iron alloys in planetary interiors, we presented X-ray absorption spectroscopy of iron–nitrogen and iron–carbon alloys at high pressures up to 50 GPa. Together with existing literature on iron–carbon, –hydrogen alloys, we analyzed their edge positions and found no significant difference in the degree of oxidation among these alloys. Pressure effects on edge positions were also found negligible. Our theoretical simulation of the valence state of iron, alloyed with S, C, O, N, and P also showed nearly unchanged behavior under pressures up to 300 GPa. This finding indicates that the high pressure bonding of iron alloyed with light elements closely resembles bonding at the ambient conditions. We suggest that the chemical properties of light elements constrain which ones can coexist within iron alloys.

Keywords: Earth's core; planetary core; light element; nitrogen; carbon; iron alloy; high pressure; X-ray absorption; XANES; Advanced Photon Source

Citation: Yang, H.; Wang, W.; Mao, W.L. Iron Bonding with Light Elements: Implications for Planetary Cores Beyond the Binary System. *Crystals* **2024**, *14*, 1016. https://doi.org/10.3390/cryst14121016

Academic Editor: Juan Ángel Sans

Received: 29 October 2024
Revised: 19 November 2024
Accepted: 20 November 2024
Published: 23 November 2024

1. Introduction

The model of Earth and terrestrial planetary cores requires an iron–light element mixture to accommodate variable observations. For Earth, the addition of light elements reduces the density and elastic moduli from pure iron to a value close to the seismic PREM profile [1]. The Earth's dynamo also requires chemical buoyancy in the outer core as an energy source. Recently, the superionic nature of ultra-high pressure iron alloys was discovered, and this can explain the softened shear modulus of Earth's inner core [2]. For the Martian core, Fe-S alloys have been used to model its compositional evolution, while the addition of other light elements is highly probable. The cores of other terrestrial planets or rocky bodies are also likely composed of iron and multiple light elements.

The candidate light elements in the core are also life-essential elements. From the perspective of planet habitability, it is important to maintain a suitable amount of these elements in near-surface reservoirs (upper crust, ocean, and atmosphere, if conditions permit). During the formation of an Earth-like planet, core segregation must have incorporated a significant amount of light elements. The relative abundance of light elements stored in the core, is a consequence of interaction of relevant components at core formation conditions.

These elements, with varied electronegativities, would suppress or facilitate the accommodation of other elements in atomic sites in either metallic melts or solids. Therefore, the competition between staying in the silicate mantle or sinking to the core can be crucial for planet habitability. A first step toward solving this problem will be understanding the oxidizing/reducing trend of light elements at core formation relevant high pressures.

The associated changes in physical properties due to light element alloying are relatively well understood, in terms of density, elastic moduli and viscosity (e.g., [3–7]). However, their effects are relatively similar, originating from their 'light' mass. From constraints of density, shear and compressional velocities, it is hard, if not impossible, to determine a multicomponent Earth core model, as the light elements can be interchangeable [8]. Alternatively, the combination of light elements could possibly be considered from a chemical perspective. The affinity of light elements to metallic iron at high pressures has been demonstrated in core formation processes, though mostly in Fe-X binary systems. However, how the valence state of iron has been altered was not well understood. The various light elements have electronegativity ranging from 1.90 (Si) to 3.44 (O). This potentially indicates the sharing of their valence electrons, which could be related to their bonding strengths with iron.

Meanwhile, the chemical identity of the bonding is not yet fully understood, especially how they can be categorized as a metallic, covalent, or ionic type of bonding. The nature of metallic planetary cores is likely to be multi-component [9]. Therefore, the compatibility of elements coexisting in the iron alloy system needs to be considered. It seems that light elements with close electronegativities become competitive when alloyed with iron. Yet, how this behavior varies with pressure remains to be understood. Knowledge of the bonding types for various light elements with iron may shed light on the behavior of ternary and polynary iron alloy systems.

X-ray Absorption Near Edge Structure spectrum is a powerful tool to detect the valence structure of transition metals in their compounds. It probes the density of states of K shell electrons by exciting electrons to the lowest empty states through X-rays with corresponding energy. The absorption edge position is sensitive to the oxidation state, and the position of the iron edge indicates how oxidized Fe atoms are. The valence state of iron is defined as the difference between the 26 electrons in a neutral iron atom and the number of electrons remaining after it loses electrons to form its current ionic state, which can be inferred either experimentally or theoretically.

In this study, we measured iron K-edge XANES spectra of iron–nitrogen and iron–carbon alloys at high pressures up to 50 GPa. We chose these compositions because carbon and nitrogen are highly siderophile during core formation, with over 90% of Earth's carbon and nitrogen stored in the core [9]. In addition to experimental results, we also employed Density Functional Theory (DFT) to calculate the valence of iron in iron–light element compounds to up to 300 GPa. Theoretical methods allow us to explore higher pressures and more compositions in the iron alloy system. We found a negligible effect of pressure on iron alloyed with light elements. As such, the iron valence state known at ambient conditions can be extrapolated to deep planetary conditions.

2. Methodology

High purity (99.9%) ε-Fe_7N_3 (Fe_3N_x, x = 1.33) and γ′-Fe_4N powders were obtained from Kojundo Chemical Lab. Co., Ltd. (Sakado, Japan)., with an average grain size of ~1 μm [10] (Figure 1). $Fe_{69}C$ (Fe-0.31 wt% C) alloy was from high-pressure temperature-treated NIST 19H basic electric steel, and $Fe_{15}C$ (Fe-1.37 wt% C) alloy was synthesized at 1 GPa and 1150 °C from a mixture of pure iron powder and an NIST 5 m Cast Iron with a 1:1 ratio. These two Fe-C alloys have very low carbon content, so the iron lattice is isostructural to pure iron, while carbon resides in the interstitial space [11]. The low carbon content also appears to have an indiscernible effect on the pressure range of the bcc-hcp phase transformation [12]. Further details of the synthesis and sample characterizations can be found in [12]. Our study focuses on the examination of iron valence

state in these alloys, with structural, strength, and spin state results for the same samples available in [10,11,13,14].

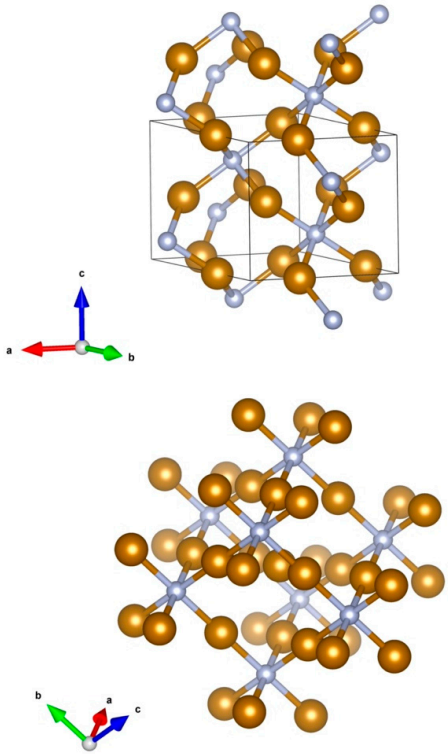

Figure 1. Crystal structure of Fe_3N_x and Fe_4N: Brown atoms represent Fe, while the light steel blue atoms represent N. Iron atoms in Fe_3N_x adopt the hexagonal closed packing, while, in the Fe_4N structure, their arrangement is the cubic closed packing. The structure data are from [12]. Crystal structure visualization was constructed by VESTA software ver. 3 [15].

These iron alloys were pre-compressed to ~15–20 μm in thickness and 50–80 μm in diameter and then loaded into sample chambers. The sample chamber is a hole of 100 μm drilled in a stainless steel gasket pre-indented to 30–40 μm in thickness. The culet size of diamond anvils is 300 μm in diameter. Silicone oil was loaded as a pressure-transmitting medium and ruby spheres were loaded as pressure calibrant.

Fe K-edge XANES spectra were measured at 13-ID-E of GSECARS at the Advanced Photon Source, Argonne National Lab. Transmission geometry was used for spectrum collection (Figure 2). Energy was scanned from 7000 eV to 7100 eV with a step size of 2.5 eV, from 7100 eV to 7130 eV with a step size of 0.1 eV. 7130 eV to 7200 eV with a step size of 1/Å in k-space. A total of 3–5 spectra were summed up to increase the signal-to-noise-ratio for high-pressure datasets. X-ray energy was calibrated by an iron foil X-ray absorption spectrum, and the peak position of the first energy derivative (E_0, where $d\mu/dE = 0$ and μ is the absorption coefficient) was calibrated to 7112 eV. The raw XAS spectra were processed using an XAS viewer (a module in Larch, http://xraypy.github.io/xraylarch/, accessed on 22 November 2024) for background removal and normalization.

To further explore the pressure effects beyond the highest pressures reached in experiments, we performed first-principle simulations based on the density functional theory (DFT) using the Vienna Ab initio Simulation Package (VASP) with the projector-augmented wave (PAW) method [16]. For the exchange-correlation functional, we used the generalized gradient approximation (GGA) [17] with the Perdew–Burke–Ernzerhof (PBE) parameterization and applied PBE pseudopotentials in our calculation. The energy cutoff was set at 600 eV. The K-point grid used for Brillouin zone summations over the electronic states was adjusted according to the structure size of individual iron alloys. We assessed the effect of the K-point mesh grid on the energy of iron alloys and found that the energy differ-

ences between the calculations with the chosen K-point mesh grid and denser grids were minimal (less than 0.05 meV/atom). We calculated a range of iron compounds including FeO, FeS, FeS_2, Fe_3C, Fe_3S, Fe_3N, and Fe_3P at 60, 100, and 300 GPa. At these pressures, these materials were expected to be non-ferromagnetic [18] so performing computation without dealing with magnetic interactions can be considered valid. After the relaxation of the cell parameters and the atomic positions of iron alloys at each pressure, we calculated the atomic valence state of Fe and other light elements from the electron charge density, following the Bader charge division scheme [19,20].

3. Results

Electrons in iron with higher valence states are bonded more strongly and require more energy to excite. As a result, the X-ray absorption edge position is associated with the oxidation state of iron (Figure 2). In Figure 3a, we compared the XANES data of common iron oxides and sulfides. At ambient conditions, metallic, ferrous, and ferric iron have distinctive edge positions (7112.5 eV, 7118 eV, and 7122 eV, respectively) though the bonded light elements are different. Based on this finding, the measured iron–nitrogen and carbon alloys are all 0 valence and do not show any oxidation features (Figure 3). The edge positions of alloys with different carbon contents are also not distinguishable (Figure 3).

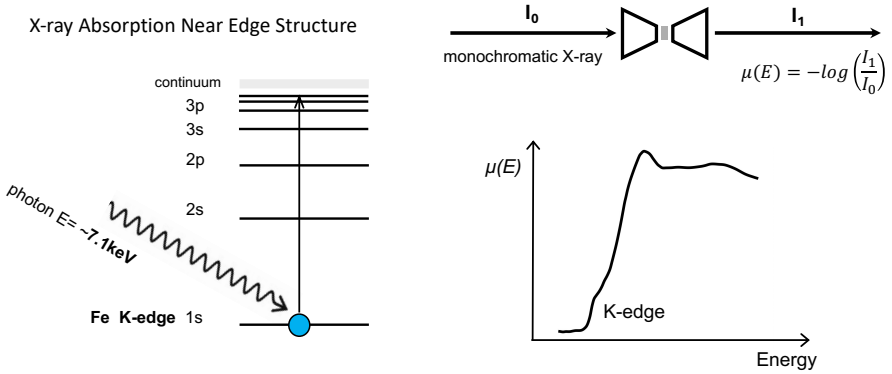

Figure 2. Schematics of principles of X-ray absorption near edge structure (XANES) and its high-pressure measurement with a diamond anvil cell. When the energy of the incident X-rays matches or exceeds the binding energy of a core electron (K-edge), the X-ray can be absorbed by an Fe atom, causing the core electron to be ejected from its shell. The absorption coefficient as a function of energy is the so-called 'near edge structure'. For high pressure experiments, the X-ray is also absorbed by the diamond anvils at both the upstream and downstream sides, resulting in lower data quality compared to ambient conditions (Figure 4).

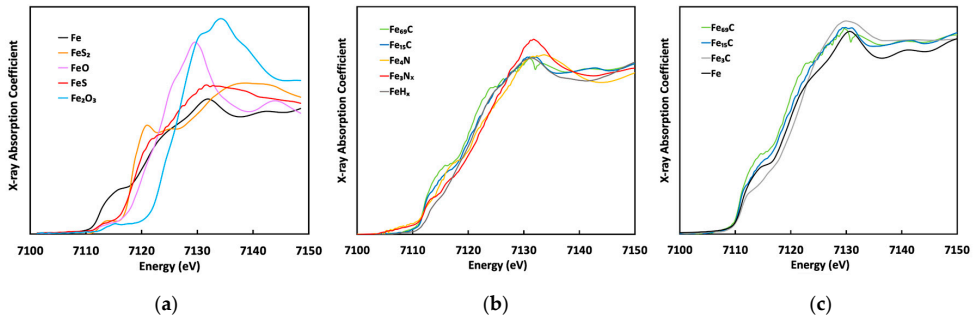

Figure 3. Fe K-edge X-ray absorption near-edge spectra of (a) common iron compounds with 0, +2 and +3 valence states, (b) iron–carbon, –nitrogen, and –hydrogen alloys at ambient conditions (except for iron–hydrogen alloy at 4 GPa), and (c) iron carbides in comparison with metallic iron. Iron-hydrogen alloy FeHx data and iron carbide Fe3C data were taken from [21,22]. FeHx shows a slightly oxidized feature compared to Fe-N and Fe-C alloys, but its edge position is still far from that of ferrous iron.

The high-pressure datasets of Fe-C and Fe-N alloys up to 56 GPa show nearly the same edge positions with the alloy at ambient conditions (Figure 4). Due to poor data quality, it is difficult to comment on the pressure-induced changes in the XANES feature other than the absorption edge. In any case, no evidence indicates that these iron alloys became ferrous (Figure 3a) so we interpret them as metallic 0-valence iron, to the highest pressure. The trend of unchanged edge positions under pressure was supported by our theoretical simulations (Figure 5). This observation is also valid for Fe-P, Fe-O, and Fe-S systems (Figure 5).

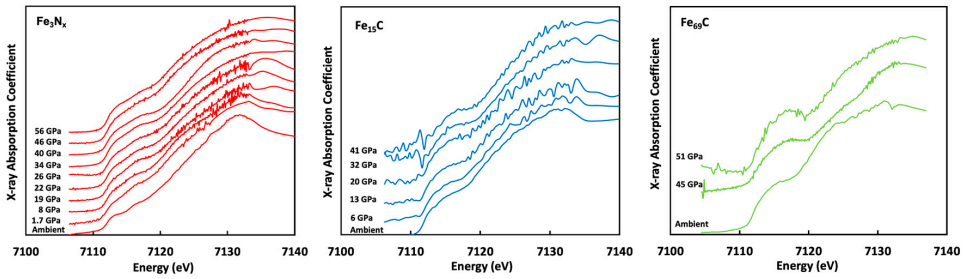

Figure 4. High pressure XANES spectra of iron–carbon and iron–nitrogen alloys. Overall, the edge positions of these alloys under high pressures remain unchanged, though some detailed features do change under pressure, which is related to pressure modification of the density of states of unfilled electron bands.

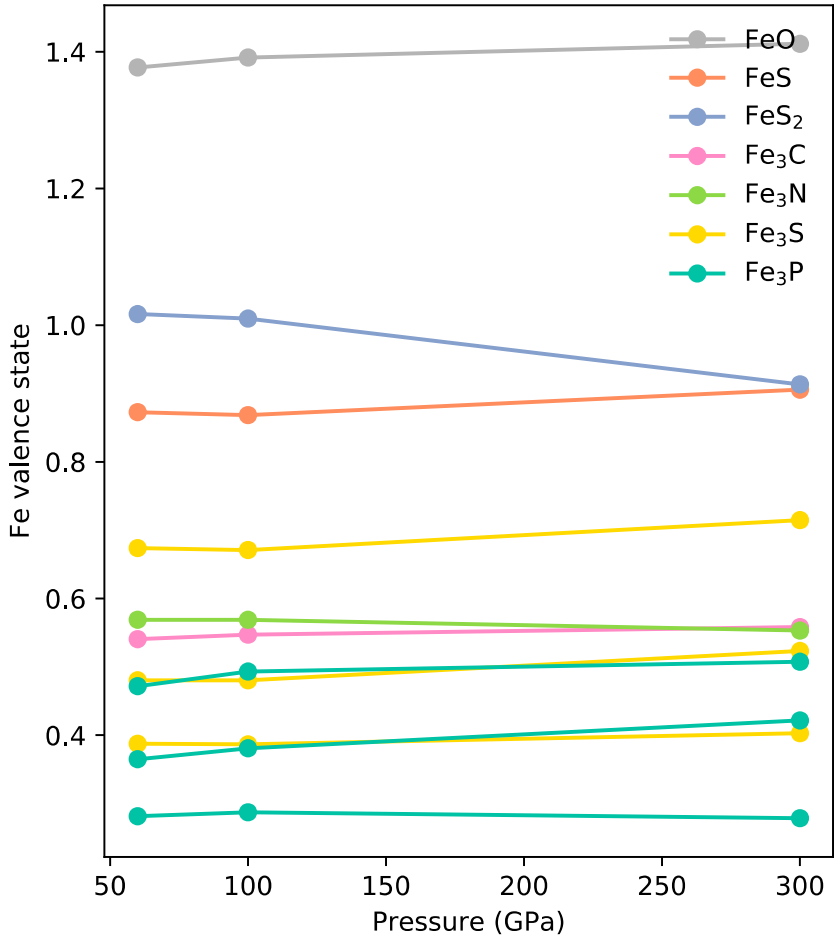

Figure 5. Valence state of iron in iron alloys calculated using Bader charge division scheme. The simulation results show no significant change in iron valence states up to 300 GPa. Based on the iron valence states, the oxidizing feature of these elements can be ranked as O > S > C ≈ N > P.

4. Discussion

Based on our results, the oxidizing or reducing characteristics of the light elements appear stable and can likely be extrapolated to high pressures up to Earth's core conditions. While planetary interiors are subject to both high pressures and temperature, previous studies on high-temperature iron alloys have shown minimal effects on the XANES edge feature [23]. Thus, we suggest that, to a first approximation, both pressure and temperature exert limited influence on the charge distribution within iron alloy systems. This stability supports our inference of consistent chemical behavior under core-like conditions. Therefore, the behavior of high-pressure ternary iron–alloy systems can be understood using the ambient condition chemical electronegativities.

If two reducing light elements are in the iron–alloy system, these two elements will be mutually exclusive above certain concentrations. For example, Fe_3C has been found not reacting with H up to 14 GPa [24]. At higher pressure, carbon in iron carbide Fe_3C was expelled by hydrogen at 43 GPa and 1900 K, forming iron hydride and diamond [25]. In the liquid iron–alloy system, the hydrogen in iron was also found to limit its carbon solubility [26]. The Fe-Si-H system has similar trends, but the behavior is more complicated due to structural complexities of iron silicide. One report showed that the Fe-Si-H compound has a composition close to $Fe_5Si_3H_3$ [27], with a H/Fe ratio lower than the typical value of $\geq$1 found in iron hydrides. This can be explained by the competing effect of Si and H in this iron–alloy system. The immiscibility of molten Fe-C and Fe-S alloys was observed below 5.5 GPa [28]. The mutual solubility of C and Si in solid hcp iron is also found to be low, and the main solid phases are FeSi and Fe_7C_3 [29]. Similarly, S and P do not coexist in a solid phase; instead, they form sulfide and phosphide when crystallization occurs [30].

We can also make an inference that reducing elements cannot coexist with oxygen in large quantities in iron alloys. This means that a separate phase of the light element oxide will crystallize from the metallic phase. Due to the significant density difference in oxides compared to metals, this leads to stratifications and release of gravitational potential energy. An example is the exsolution of SiO_2 in Fe-Si-O system at high pressures [31], which can gradually change the liquid core composition and provide an energy source for powering the dynamo, especially during Earth's early stage. In addition, Mg oxide exsolution [32,33] from liquid outer core has also been proposed as an energy source for the early dynamo. Because increasing the oxygen content in the core with reducing elements would drive the exsolution of oxides from the iron–alloy system, the oxygen content becomes a critical limit of light element's solubility in the core.

Our XAS data provide benchmarks of the absorption edge of Fe alloys. This could be potentially useful to determine the composition of high-pressure iron alloys during partial melting, especially for experiments performed in diamond anvil cells. The partition between solid and liquid phases would result in chemical gradients in light elements, which could be potentially resolved using the XANES method, given the light elements vary in electronegativity, and the spectra data are of high quality. The presented data here may be also applicable to iron meteorite characterizations or spectroscopic observation of asteroids or planets with a primarily metallic surface.

5. Conclusions

In summary, we present a combined experimental and theoretical approach, which offers a perspective for understanding charge distribution and oxidation states in iron alloys under extreme conditions. Specifically, we report XANES spectra of $Fe_{15}C$, $Fe_{69}C$, and Fe_3N_x at high pressures up to 50 GPa. The absorption edge position of iron K-edge remains unchanged in the investigated pressure range. We further calculated the valence state of iron alloys using first-principle density functional theory up to 300 GPa and found nearly unchanged iron valence states. This indicates the relative electronegativity for Fe-C, Fe-N, Fe-S, Fe-O, and Fe-P, and, hence, the bonding nature was not significantly changed by pressure. The similar bounding nature of iron alloys at ambient conditions and high pressures indicates the 'oxidizing' and 'reducing' features of these elements remain

valid at high pressures and can be used to explain the ternary iron alloy behaviors at high pressures. These insights contribute to predicting planetary core compositions and behaviors, providing practical implications for planetary science and interior modeling. Applying this knowledge, we illustrate the repulsive interaction of C and H in Fe-C-H systems and the SiO_2 crystallization behavior in Fe-Si-O system.

Future studies could expand on this work by examining a broader range of light elements, taking XAS measurement on light elements C, O, or S, incorporating higher temperatures to simulate a wider range of planetary environments, as well as exploring ternary systems to assess multi-element interactions more directly. This approach would help refine our understanding of core composition and the conditions that affect core-mantle differentiation across diverse planetary bodies.

Author Contributions: Conceptualization, H.Y. and W.L.M.; methodology, H.Y., W.W. and W.L.M.; software, H.Y. and W.W.; validation, H.Y., W.W. and W.L.M.; formal analysis, H.Y. and W.W.; investigation, H.Y. and W.W.; resources, W.W. and W.L.M.; data curation, H.Y. and W.W.; writing—original draft preparation, H.Y.; writing—review and editing, H.Y., W.W. and W.L.M.; visualization, H.Y.; supervision, W.L.M.; project administration, H.Y. and W.L.M.; funding acquisition, W.L.M. All authors have read and agreed to the published version of the manuscript.

Funding: NSF CSEDI Program (EAR2153968) and NASA Exoplanet Program (80NSSC23K0265).

Data Availability Statement: The raw and processed XANES data and valence state results from DFT simulations can be found in the open-access Zenodo repository [34].

Acknowledgments: We thank Jiachao Liu and Jing Yang for providing Fe-N alloy and Fe-C alloy samples. We appreciate Matt Newville for his valuable assistance during the experiments. We also gratefully acknowledge the Supercomputing Center of University of Science and Technology of China for providing the computational resources used in this work. Portions of this work were performed at GeoSoilEnviroCARS (The University of Chicago, Sector 13), Advanced Photon Source (APS), Argonne National Laboratory. GeoSoilEnviroCARS was supported by the National Science Foundation—Earth Sciences (EAR—1634415). This research used resources of the Advanced Photon Source, a U.S. Department of Energy (DOE) Office of Science User Facility operated for the DOE Office of Science by Argonne National Laboratory under Contract No. DE-AC02-06CH11357. We acknowledge support from the NSF CSEDI Program (EAR2153968) and NASA Exoplanet Program (80NSSC23K0265). This study originated from Chapter 2 of Yang's PhD thesis (June 2024, Stanford University), which benefited from comments from defense committee members Wendy L. Mao, Rodney C. Ewing, Sonia M. Tikoo, Laura K. Schaefer, and Anton I. Ermakov. We appreciate comments from three anonymous reviewers that greatly improved our manuscript.

Conflicts of Interest: The authors declare no conflict of interest.

References

1. Brown, J.M.; Shankland, T.J. Thermodynamic parameters in the Earth as determined from seismic profiles. *Geophys. J. Int.* **1981**, *66*, 579–596. [CrossRef]
2. Wang, W.; Li, Y.; Brodholt, J.P.; Vočadlo, L.; Walter, M.J.; Wu, Z. Strong shear softening induced by superionic hydrogen in Earth's inner core. *Earth Planet. Sci. Lett.* **2021**, *568*, 117014. [CrossRef]
3. Mao, Z.; Lin, J.-F.; Liu, J.; Alatas, A.; Gao, L.; Zhao, J.; Mao, H.-K. Sound Velocities of Fe and Fe-Si Alloy in the Earth's Core. *Proc. Natl. Acad. Sci. USA* **2012**, *109*, 10239–10244. [CrossRef] [PubMed]
4. Liu, J.; Lin, J.-F.; Alatas, A.; Bi, W. Sound Velocities of Bcc-Fe and Fe0.85Si0.15 Alloy at High Pressure and Temperature. *Phys. Earth Planet. Inter.* **2014**, *233*, 24–32. [CrossRef]
5. Badro, J.; Brodholt, J.P.; Piet, H.; Siebert, J.; Ryerson, F.J. Core Formation and Core Composition from Coupled Geochemical and Geophysical Constraints. *Proc. Natl. Acad. Sci. USA* **2015**, *112*, 12310–12314. [CrossRef]
6. Zhang, Y.; Sekine, T.; Lin, J.-F.; He, H.; Liu, F.; Zhang, M.; Sato, T.; Zhu, W.; Yu, Y. Shock Compression and Melting of an Fe-Ni-Si Alloy: Implications for the Temperature Profile of the Earth's Core and the Heat Flux Across the Core-Mantle Boundary. *J. Geophys. Res. Solid Earth* **2018**, 2017JB014723. [CrossRef]
7. Zhu, F.; Lai, X.; Wang, J.; Williams, Q.; Liu, J.; Kono, Y.; Chen, B. Viscosity of Fe-Ni-C Liquids up to Core Pressures and Implications for Dynamics of Planetary Cores. *Geophys. Res. Lett.* **2022**, *49*, e2021GL095991. [CrossRef]
8. Hirose, K.; Wood, B.; Vočadlo, L. Light elements in the Earth's core. *Nat. Rev. Earth Environ.* **2021**, *2*, 645–658. [CrossRef]
9. McDonough, W.F. Compositional Model for the Earth's Core. In *Treatise on Geochemistry*, 2nd ed.; Holland, H.D., Turekian, K.K., Eds.; Elsevier: Oxford, UK, 2014; ISBN 978-0-08-098300-4.

10. Lv, M.; Liu, J.; Zhu, F.; Li, J.; Zhang, D.; Xiao, Y.; Dorfman, S.M. Spin Transitions and Compressibility of ε-Fe7N3 and γ′-Fe4N: Implications for Iron Alloys in Terrestrial Planet Cores. *J. Geophys. Res. Solid Earth* **2020**, *125*, e2020JB020660. [CrossRef]
11. Yang, J.; Fei, Y.; Hu, X.; Greenberg, E.; Prakapenka, V.B. Effect of Carbon on the Volume of Solid Iron at High Pressure: Implications for Carbon Substitution in Iron Structures and Carbon Content in the Earth's Inner Core. *Minerals* **2019**, *9*, 720. [CrossRef]
12. Jacobs, H.; Rechenbach, D.; Zachwieja, U. Structure determination of γ′-Fe4N and ε-Fe3N. *J. Alloys Compd.* **1995**, *227*, 10–17. [CrossRef]
13. Zhuang, Y.; Liu, J.; Lv, C.; Xu, L.; Bi, W.; Hu, Q.; Zhang, D.; Garbarino, G.; Zhu, S.; Zhang, Y. Magnetic collapse and low conductivity of Fe3N in the deep interiors of Earth-like planets. *Am. Mineral.* 2024. [CrossRef]
14. Pease, A.; Liu, J.; Lv, M.; Xiao, Y.; Armstrong, K.; Popov, D.; Miyagi, L.; Dorfman, S.M. Strength, Plasticity, and Spin Transition of Fe-N Compounds in Planetary Cores. *Phys. Earth Planet. Inter.* **2024**, *355*, 107236. [CrossRef]
15. Momma, K.; Izumi, F. VESTA3 for three-dimensional visualization of crystal, volumetric and morphology data. *J. Appl. Crystallogr.* **2011**, *44*, 1272–1276. [CrossRef]
16. Blöchl, P.E. Projector augmented-wave method. *Phys. Rev. B* **1994**, *50*, 17953–17979. [CrossRef] [PubMed]
17. Perdew, J.P.; Burke, K.; Ernzerhof, M. Generalized Gradient Approximation Made Simple. *Phys. Rev. Lett.* **1996**, *77*, 3865–3868. [CrossRef]
18. Dewaele, A.; Nataf, L. Magnetic phase diagram of iron at high pressure and temperature. *Phys. Rev. B* **2022**, *106*, 014104. [CrossRef]
19. Bader, R.F.W.; Henneker, W.H.; Cade, P.E. Molecular Charge Distributions and Chemical Binding. *J. Chem. Phys.* **1967**, *46*, 3341–3363. [CrossRef]
20. Yu, M.; Trinkle, D.R. Accurate and efficient algorithm for Bader charge integration. *J. Chem. Phys.* **2011**, *134*, 064111. [CrossRef]
21. Bouldi, N. Electronic and magnetic properties of iron hydride under pressure: An experimental and computational study using x-ray absorption spectroscopy and x-ray magnetic circular dichroism at the Fe K edge. *Phys. Rev. B* **2018**, 8. [CrossRef]
22. Meng, Y.; Newville, M.; Sutton, S.; Rakovan, J.; Mao, H.-K. Fe and Ni impurities in synthetic diamond. *Am. Mineral.* **2003**, *88*, 1555–1559. [CrossRef]
23. Boccato, S.; Torchio, R.; Anzellini, S.; Boulard, E.; Guyot, F.; Irifune, T.; Harmand, M.; Kantor, I.; Miozzi, F.; Parisiades, P.; et al. Melting Properties by X-Ray Absorption Spectroscopy: Common Signatures in Binary Fe–C, Fe–O, Fe–S and Fe–Si Systems. *Sci. Rep.* **2020**, *10*, 11663. [CrossRef] [PubMed]
24. Terasaki, H.; Shibazaki, Y.; Nishida, K.; Tateyama, R.; Takahashi, S.; Ishii, M.; Shimoyama, Y.; Ohtani, E.; Funakoshi, K.; Higo, Y. Repulsive Nature for Hydrogen Incorporation to Fe3C up to 14 GPa. *ISIJ Int.* **2014**, *54*, 2637–2642. [CrossRef]
25. Lai, X.; Zhu, F.; Gao, J.; Greenberg, E.; Prakapenka, V.B.; Meng, Y.; Chen, B. Melting of the Fe-C-H System and Earth's Deep Carbon-Hydrogen Cycle. *Geophys. Res. Lett.* **2022**, *49*, e2022GL098919. [CrossRef]
26. Hirose, K.; Tagawa, S.; Kuwayama, Y.; Sinmyo, R.; Morard, G.; Ohishi, Y.; Genda, H. Hydrogen Limits Carbon in Liquid Iron. *Geophys. Res. Lett.* **2019**, *46*, 5190–5197. [CrossRef]
27. Fu, S.; Chariton, S.; Prakapenka, V.B.; Chizmeshya, A.; Shim, S.-H. Stable hexagonal ternary alloy phase in Fe-Si-H at 28.6–42.2 GPa and 3000 K. *Phys. Rev. B* **2022**, *105*, 104111. [CrossRef]
28. Corgne, A.; Wood, B.J.; Fei, Y. C- and S-rich molten alloy immiscibility and core formation of planetesimals. *Geochim. Cosmochim. Acta* **2008**, *72*, 2409–2416. [CrossRef]
29. Miozzi, F.; Morard, G.; Antonangeli, D.; Baron, M.A.; Pakhomova, A.; Clark, A.N.; Mezouar, M.; Fiquet, G. The Fe-Si-C system at extreme P-T conditions: A possible core crystallization pathway for reduced planets. *Geochim. Cosmochim. Acta* **2022**, *322*, 129–142. [CrossRef]
30. Zhai, K.; Yin, Y.; Zhai, S. New constraints on the abundances of phosphorus and sulfur in the lunar core: High-pressure and high-temperature experimental study of the Fe-S-P ternary system. *Geochim. Cosmochim. Acta* **2022**, *334*, 1–13. [CrossRef]
31. Hirose, K.; Morard, G.; Sinmyo, R.; Umemoto, K.; Hernlund, J.; Helffrich, G.; Labrosse, S. Crystallization of silicon dioxide and compositional evolution of the Earth's core. *Nature* **2017**, *543*, 99–102. [CrossRef]
32. O'Rourke, J.G.; Stevenson, D.J. Powering Earth's dynamo with magnesium precipitation from the core. *Nature* **2016**, *529*, 387–389. [CrossRef] [PubMed]
33. Deng, J.; Du, Z. Primordial helium extracted from the Earth's core through magnesium oxide exsolution. *Nat. Geosci.* **2023**, *16*, 541–545. [CrossRef]
34. Yang, H.; Wang, W.; Mao, W. *Iron Bonding with Light Elements: Implications for Planetary Cores Beyond the Binary System [Data Set]*; Zenodo: Geneva, Switzerland, 2024. [CrossRef]